Spherical nucleic acids for topical treatment of hyperpigmentation

Yang Fang, Xueguang Lu, Dali Wang, Jiansong Cai, Yuyan Wang, Peiru Chen, Mengqi Ren, Hao Lu, Jennifer Union, Lei Zhang, Yehui Sun, Fei Jia, Xi Kang, Xuyu Tan[1,2]*, and Ke Zhang[1]*

1. Department of Chemistry and Chemical Biology, Northeastern University, Boston, Massachusetts 02115, United States

2. Department of Chemistry, Massachusetts Institute of Technology, 77 Massachusetts Avenue, Cambridge, Massachusetts 02139, United States

ABSTRACT: Oligonucleotide-based materials such as spherical nucleic acid (SNA) have been reported to exhibit improved penetration through the epidermis and the dermis of the skin upon topical application. Herein, we report a self-assembled, skin-depigmenting SNA structure, which is based upon a bifunctional oligonucleotide amphiphile containing an antisense oligonucleotide and a tyrosinase inhibitor prodrug. The two components work synergistically to increase oligonucleotide cellular uptake, enhance drug solubility, and promote skin penetration. The particles were shown to reduce melanin content in B16F10 melanoma cells and exhibited potent anti-melanogenic effect in an ultraviolet B-induced hyperpigmentation mouse model.

Hyperpigmentation, a common condition associated with exposure to ultraviolet (UV) light or skin inflammation, occurs when excess melanin forms deposits in the skin.[1] Melanogenesis takes place in melanocytes, which are located at the basal layer of the epidermis.[2] It is mainly regulated by tyrosinase (TYR) and other tyrosinase-related proteins (TRPs).[3-4] These enzymes are transcriptionally regulated by the microphthalmia-associated transcription factor (MITF).[5] Melanin biosynthesis can be stimulated with the increased production of MITF, which is a result of melanocortin 1 receptor (MC1R) binding to the α-melanocyte-stimulating hormones (α-MSHs).[6-8] Current treatments for hyperpigmentation include physical means such as laser/chemical skin resurfacing and microdermabrasion, which need to be carefully managed to minimize skin damage,[9] and transdermal delivery of TYR inhibitors. The latter is a less invasive and more convenient alternative that does not interfere with the patient's normal daily life.

Commonly used TYR inhibitors include kojic acid, phenylethyl resorcinol, and hydroquinone, which perform well *in vitro* but suffer from side-effects such as skin irritation and/or limited absorption.[10-11] Phenylethyl resorcinol (PR), a particularly potent TYR inhibitor,[12] which inhibits mushroom tyrosinase ~22 times more effectively than kojic acid,[13] has been adopted as the active ingredient in depigmenting commercial products.[14] However, the poor aqueous solubility of PR reduces skin absorption and overall efficacy.[14] Attempts to target upstream proteins using anti-MITF or anti-MC1R siRNA together with a transdermal peptide have been shown to deplete target transcripts and produce a skin-lightening effect on patients with hyperpigmented facial lesions after 12 weeks of topical treatment.[15] However, efficient topical delivery of oligonucleotide drugs across intact skin remains a lasting challenge due to the stratum corneum ,[16] which is a strong barrier of the epidermis that impedes a wide range of agents intended for the skin.[17-19] Recently, spherical nucleic acids (SNAs), which are core-shell nanoparticles with a densely functionalized oligonucleotide shell and a rigid core (metallic or non-metallic particles), have been shown to penetrate the skin barrier and abolish target gene expression in the epidermis and dermis with only three weeks of topical treatment in the absence of a transfection agent.[20-21]

Scheme 1. Structure of ASO-PR$_{10}$ prodrug conjugate and their micellar SNA assembly. Upon skin penetration, bioactive PR and ASO are released.

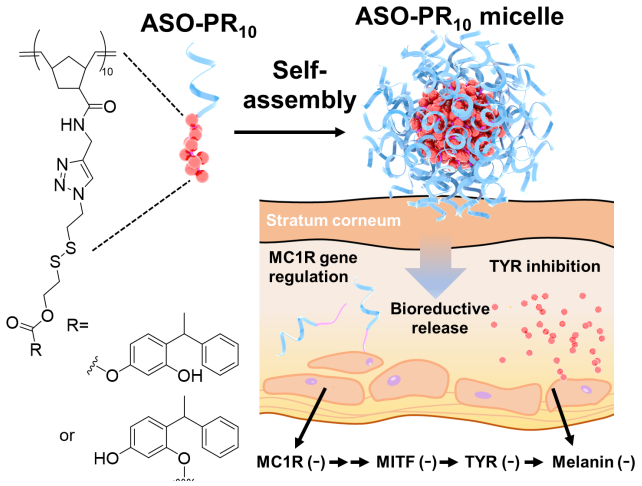

Here, we report an SNA-based skin depigmentation agent incorporating an antisense oligonucleotide (ASO) targeting MC1R (to downregulate new TYR synthesis) and a polymerized PR prodrug, which releases active PR bioreductively upon cell internalization (to disable existing TYR).

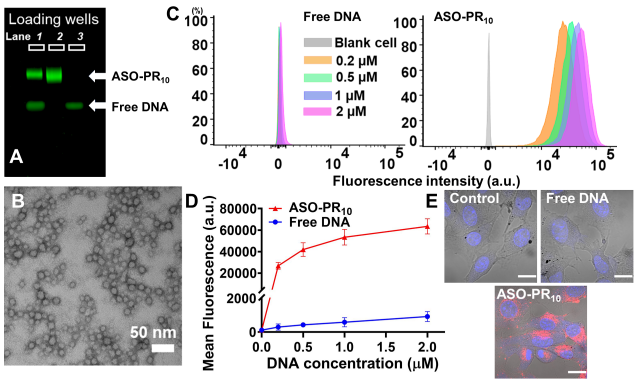

Figure 1 A) Agarose gel (2%) electrophoresis of the conjugation reaction mixture (lane 1) between N_3-PR_{10} and DBCO-ASO, purified ASO-PR_{10} conjugate (lane 2), and free ASO (lane 3). **B)** TEM image of the ASO-PR_{10} nanoparticles. Samples were stained with uranyl acetate (2%). **C,D)** Flow cytometry measurement of B16F10 cells treated with Cy5-labeled ASO-PR_{10} SNAs or Cy5-labeled free ASO (0.2-2 μM ASO, 4 h), showing significantly (>100×) higher uptake for the SNAs. Error bar: mean ± SD; n = 3. **E)** Confocal microscopy imaging of cells treated with 2 μM of Cy5-labeled ASO-PR_{10} nanoparticles or free ASO. Images taken with identical settings. Scale bar: 20 μm.

The SNA takes advantage of the amphiphilicity of the ASO-drug conjugate,[22-23] allowing for the formation of a spherical micelle with a dense DNA shell which is structurally analogous to prototypical SNAs (Scheme 1). The ASO component functions as both a carrier and a payload, enhancing drug water solubility and transdermal delivery of both components while being an active agent for gene regulation. It has been shown that the antisense SNAs regulate gene expression by RNase H-mediated degradation of target mRNA without the ASO being released.[24]

The amphiphile is assembled by copper-free click chemistry using an ASO modified with a 5' dibenzocyclooctyne (DBCO) and an azide-functionalized prodrug polymer (Scheme S1). Because of the lack of an established MC1R ASO sequence, we screened a number of sequences against the MC1R mRNA in murine melanoma B16F10 cells using lipofectamine 2k-formulated ASOs, and identified a sequence with reasonable antisense activity (sequence:5'-TTCTCCACCAGACTCACCA-3', Figure S1).[25-27] The polymer is synthesized via sequential ring opening metathesis polymerization of two monomers, an oxanorbornene bromide (N-Br)[28] and a norbornene disulfide PR (N-SS-PR),[23] which gives a narrowly dispersed diblock copolymer (PDI=1.2, M_w=7.0 kDa, Figure S2) with high yield (~98%). Azide substitution of the bromide is carried out post-polymerization. A bioreductive, self-immolative disulfide linker is incorporated in N-SS-PR,[29] which can be cleaved under intracellular reductive conditions and release the active form of the drug. The ratio between PR and DNA is designed to be 10:1 (mol:mol) by controlling the stoichiometries during polymerization and final coupling. This ratio is balanced to provide sufficient driving force for micellization while also maintaining solubility during polymerization and coupling. The coupling reaction is performed in dimethylformamide (DMF):water (5:1, v:v) mixture, giving a yield of ~68% based on gel electrophoresis band densitometry analysis (Figure 1A).

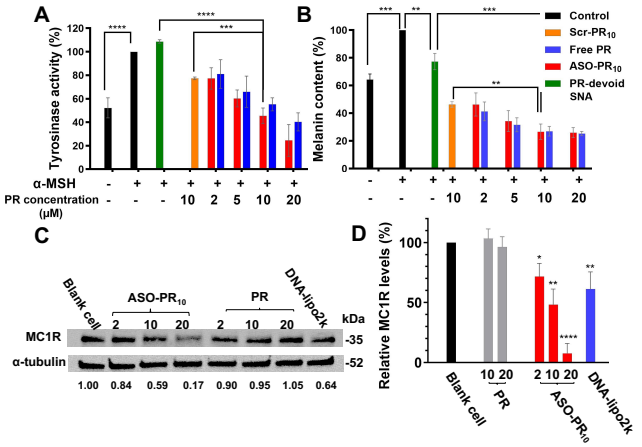

Figure 2. Tyrosinase activity **A)** and melanin content **B)** upon treatment with ASO-PR_{10}, DNA-PR_{10} with a scrambled sequence (Scr-PR_{10}), PR-devoid micelles (in PBS), or free PR (in DMSO). α-MSH is used stimulate melanogenesis. Tyrosinase activity and melanin content are recorded as percent changes compared with α-MSH-treated cells (2 to 20 μM PR, 48 h treatment). PR-devoid micelles: 1 μM ASO. **C,D)** MCIR levels in B16F10 cells after treatment with PR, ASO-PR_{10}, and controls (2 to 20 μM PR, 72 h treatment) as determined by western blot analysis. DNA-lipofectamine2k complexes: 10 μM ASO. *p<0.05, **p<0.01, ***p<0.001, ****p<0.0001 (two-tailed test).

The ASO-PR_{10} amphiphile readily forms spherical micellar nanoparticles in an aqueous buffer. Dynamic light scattering shows the presence of nanoparticles with a number-average hydrodynamic diameter of 18.4 ± 5.2 nm (Figure S3, Table S2) and a zeta potential of −21.8 ± 4.8 mV. The formation of micelles is also confirmed by transmission electron microscopy (TEM), which shows spherical particle with dry-state sizes averaging 15.2 ± 1.4 nm (Figure 1B). To test if the PR component can be released, dithiothreitol (DTT) is used to simulate the reductive intracellular environment. When treated with 10 mM DTT at 37 °C for 1-4 h, a faster-migrating band emerged during gel electrophoresis, which is likely the monomeric form of the PR-free DNA-polymer conjugate (Figure S4). The released compound matches unmodified PR in mass (measured by electrospray ionization mass spectrometry) and in retention time during reverse-phase HPLC analysis (Figure S5).

To examine the cellular uptake of the ASO-PR_{10} nanoparticles, B16F10 cells were treated with Cy5-labeled nanoparticles or free DNA in the concentration range of 0.2 to 2 μM (DNA basis). ASO-PR_{10}-treated cells exhibit ~100 times higher cellular uptake than free ASO-treated cells, as evidenced by flow cytometry (Figure 1C,D). The high level of uptake is corroborated by confocal laser scanning microscopy, which shows strong fluorescence signals in the cytoplasm of the cells treated with ASO-PR_{10} nanoparticles but only background signals for ASO- and vehicle (phosphate-buffered saline, PBS)-treated cells (Figure 1E). The high cell

uptake of SNA-type nanoparticles has been shown to be the result of class A scavenger receptors-mediated endocytosis via a lipid-raft–dependent, caveolae-mediated pathway (Figure S6).[30] Pretreatment of B16F10 cells with the pharmacological inhibitor methyl-β-cyclodextrin (which depletes and removes cholesterol) significantly reduces intracellular accumulation of Cy5-labeled ASO-PR_{10}, which is consistent with prior mechanistic studies. Despite high cellular uptake, the ASO-PR_{10} particles exhibit negligible levels of cytotoxicity in the concentration range tested 1-20 μM (PR basis), by a 3-(4,5-dimethylthiazol-2-yl)-2,5-diphenyltetrazolium bromide cytotoxicity assay (Figure S7). In addition, the cells are morphologically identical to untreated cells by microscopic evaluation.

Next, we compare the anti-melanogenic efficacy of ASO-PR_{10} nanoparticles, free PR, DNA-PR_{10} nanoparticle with a scrambled sequence (Scr-PR_{10}), and PR-devoid ASO micelles *in vitro* by measuring tyrosinase inhibition and melanin content. B16F10 cells were treated with α-MSH (200 nM) to stimulate melanin formation. When ASO-PR_{10} nanoparticles and equivalent amounts of free PR (2 to 20 μM PR) were added, the effects of α-MSH were reversed in a dose-dependent manner. Remarkably, the ASO-PR_{10} particles show comparable reduction in tyrosinase activity to molecular PR despite that the latter is able to freely diffuse into the cell (inferred from an octanol/water partition coefficient value of 3.35)[31] while the particles require bioreductive activation (Figure 2A). Furthermore, potent anti-melanogenic effect is observed for both ASO-PR_{10} and PR as determined by measuring the intracellular melanin content using light absorbance at 405 nm, corroborating the efficient intracellular release of PR in the active form by the micelles (Figure 2B, S8). To measure the antisense activity of the ASO-PR_{10} SNAs, MC1R levels from B16F10 cell lysates were measured by western blot. SNAs reduced MC1R levels in a dosage dependent manner, with a maximum reduction level (83%) achieved at 2 μM ASO (20 μM PR). The effect is not a feedback loop of released molecular PR, as PR itself does not cause changes in MC1R levels at the same PR concentration (Figure 2C,D). Interestingly, ASO-PR_{10} particles show slightly better reduction in tyrosinase activity and melanin content than both Scr-PR_{10} and PR-devoid particles, suggesting some level of synergy between the ASO and PR. Collectively, these results show that the drug and ASO components in the ASO-PR_{10} serve as an effective delivery vehicle for each other through the formation of SNAs but retain their bioactivity upon cellular uptake.

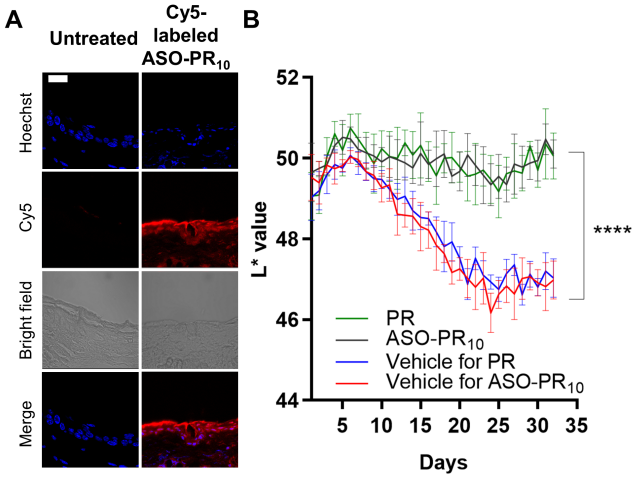

Figure 3. A) Fluorescence micrographs of mouse ear sections (paraffin-embedded) after treatment with Cy5-labeled ASO-PR_{10} (red). Cell nuclei are stained with Hoechst 33342 (blue). ASO-PR_{10} fluorescence is present throughout the stratum corneum, epidermis, and dermis. Scale bar: 20 μm. **B)** Brightness levels (L* value) in mouse left (blue/red) and right (green/black) ears upon treatment with sample/vehicle groups for 32 days. ****p<0.0001 (two-tailed test).

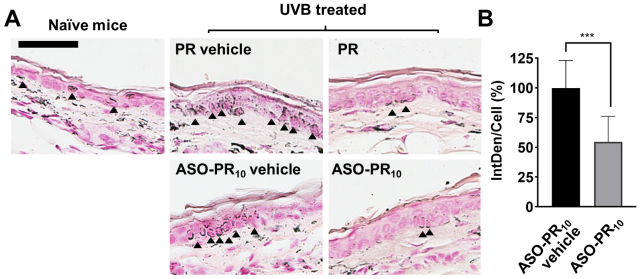

Figure 4 A) Histological analysis of sectioned mouse ear after treatment with PR/ASO-PR_{10}/vehicle groups (paraffin-embedded). Melanin (indicated by black arrows) is stained by Fontana-Masson staining. Scale bar: 50 μm. **B)** Relative MC1R levels in ASO-PR_{10}- vs. vehicle-treated mouse ears as determined by immunohistostaining. *** p<0.001 (two-tailed test).

In order to examine the degrees of skin penetration and depigmentation, C57BL/6 mice are used as a model. Because the epidermis of the mice ear skin contains epidermal melanocytes, unlike the trunk/fur-bearing skin, the ear skin region is selected for testing.[32-33] Cy5-labeled ASO-PR_{10} SNAs, Cy5-labeled free ASO, and free Cy5 dye (equivalent to 10 μM DNA, dispersed in Nanopure™ water) were topically applied to hairless ear skin every 8 hours for a total of 4 times. Fluorescence microscopy of sectioned ear skin revealed significant fluorescence in the matrix of the stratum corneum, the cytoplasm of epidermal cells, and the dermis for the ASO-PR_{10}-treated sample but not for control-treated samples (Figure 3A, S9). To test the efficacy of the SNA in suppressing melanogenesis, the SNA, PR, or vehicle was topically applied daily for 32 days to the dorsal ear skin of the mouse. To minimize differences among individuals, the right ear of each mice receives SNA or PR while the left ear is treated with an equal volume of vehicle. Due to the poor solubility of PR in water, a mixed solvent of 1,2-propanediol/ethanol (v/v 3:7) was used as vehicle, while the SNAs remain dispersed in water. On days 8 through 22, mice were exposed to 200 mJ/cm² of UVB irradiation every other day to induce hyperpigmentation (Figure S10). The degree of depigmentation is quantitatively evaluated by comparing the skin color between the two ears of mice. The skin lightness was measured in reflectance by colorimetry using a tristimulus colorimeter and shown as L*, which is the lightness component in the

CIELAB color space. The darkest black is represented by L* = 0, and the brightest white at L* = 100. The L* values of both ears of mice were recorded daily (Figure 3B). During days 8 to 22, UVB irradiation induced significant melanogenesis in both vehicle-treated groups as reflected in a decrease of L* values, with an average ΔL* of -2.9±0.5 (water) and -2.8±0.6 (1,2-propanediol/ethanol). Strikingly, the ASO-PR_{10}- and PR-treated groups both exhibited insignificant changes in L*, suggesting successful blockage of melanogenesis. Upon termination of UVB irradiation, the vehicle treated groups cease to further darken, while the ASO-PR_{10}- and PR-treated groups lighten slightly, with ΔL* being ~ +0.5±0.7 and +0.4±0.3, respectively. Overall, comparing to day 32 to day 1, both PR and SNA produced a net skin lightening effect despite UVB-irradiation for two weeks, while both control groups exhibited a visible darkening effect (Figure S11). Collectively, these results support that the PR-loaded SNA can deliver the active ingredients through the stratum corneum to induce a protective, anti-melanogenic effect and avoid hyperpigmentation upon topical application.

To further study the effect of ASO-PR_{10} on a tissue level, the distribution of melanin at the epidermis layer was visualized by Fontana-Masson staining. There is clearly a higher level of melanin in the epidermis of vehicle-treated left ear, as demonstrated by deposits of melanin (indicated by the arrows), whereas treatment by PR or ASO-PR_{10} decreased melanin content in the epidermis to levels comparable to non-treated control (Figure 4A). To test the antisense efficacy of the SNA in suppressing MC1R expression, MC1R protein was detected by immunohistochemistry (IHC) staining (Figure S12). While both vehicle- and SNA-treated tissues exhibit fluorescence associated with MC1R, the intensity for the ASO-PR_{10} is ~50% that of the vehicle-treated control (Figure 4B). However, the reduction may not have contributed to the overall phenotypic response, as the SNA does not show an advantage in activity despite having the ability to reduce MC1R levels. This observation may be due to insufficient treatment time, incomplete depletion of target protein,[15] or the fact that PR by itself can effectively suppress TYR activity once delivered to the cell. However, the poor water solubility of PR requires a harsh solvent condition to be used, which may cause skin drying and irritations. For better synergy, future designs may target alternative pathways such as MC1R-free tyrosinase biosynthesis initiated by p53.[34]

In summary, we have synthesized an SNA-like micellar nanoparticle with a tyrosinase inhibitor prodrug core and an ASO shell that can inhibit the expression of a key receptor involved in melanogenesis. This drug-cored SNA can penetrate the ear skin of mice upon direct topical application. Once inside the melanocytes, the drug component is released via cleavage of a bioreductive, self-immolative linker, while the ASO inhibits target gene expression. This approach takes advantage of otherwise weaknesses associated with highly hydrophobic drug molecules and non-cell-penetrating ASOs, and transforms them into essential features that enable their co-delivery across the skin and into skin cells. The principles demonstrated here should be broadly applicable for drug/oligonucleotide combination therapies that target a variety of skin-related disorders via topical application.

ASSOCIATED CONTENT

Supporting Information.
The Supporting Information is available free of charge on the at DOI:
Materials and methods, experimental procedures, instrumentation, supplemental figures and references

AUTHOR INFORMATION

Corresponding Author

* E-mail: k.zhang@northeastern.edu

ORCID

Ke Zhang: 0000-0002-8142-6702

Author Contributions

K.Z., Y.F. and X.T. devised the experiments and wrote the manuscript. Y.F. conducted the synthesis of materials, purification and material/biological characterization. All other authors contributed to material synthesis, purification, and/or discussion of the results. All authors edited the manuscript.

Funding Sources

Notes

The authors declare no competing financial interest.

ACKNOWLEDGMENT

This publication was made possible by the National Science Foundation (DMR award number 2004947) and the National Institute of General Medical Sciences (award number 1R01GM121612). The authors thank Dr. Heather Clark for assistance with confocal microscopy, Dr. William Fowle for electron microscopy, Dr. Jiahe Li for flow cytometer, and Dr. Roman Manetsch for mass spectrometry.

REFERENCES

1. Rigopoulos, D.; Gregoriou, S.; Katsambas, A., Hyperpigmentation and melasma, **2007,** *6* (3), 195-202.
2. D'Mello, S. A. N.; Finlay, G. J.; Baguley, B. C.; Askarian-Amiri, M. E., Signaling Pathways in Melanogenesis, *Int. J. Mol. Sci.* **2016,** *17*, 1144.
3. Kim, Y. J.; Uyama, H., Tyrosinase inhibitors from natural and synthetic sources: structure, inhibition mechanism and perspective for the future, *Cell Mol Life Sci* **2005,** *62* (15), 1707-23.
4. del Marmol, V.; Beermann, F., Tyrosinase and related proteins in mammalian pigmentation, *FEBS Lett.* **1996,** *381* (3), 165-168.
5. Chao, H.-C.; Najjaa, H.; Villareal, M. O.; Ksouri, R.; Han, J.; Neffati, M.; Isoda, H., Arthrophytum scoparium inhibits melanogenesis through the down-regulation of tyrosinase and melanogenic gene expressions in B16 melanoma cells, *Exp. Dermatol.* **2013,** *22* (2), 131-136.
6. Chiang, H.-M.; Chien, Y.-C.; Wu, C.-H.; Kuo, Y.-H.; Wu, W.-C.; Pan, Y.-Y.; Su, Y.-H.; Wen, K.-C., Hydroalcoholic extract of Rhodiola rosea L. (Crassulaceae) and its hydrolysate inhibit melanogenesis in B16Fo cells by regulating the CREB/MITF/tyrosinase pathway, *Food Chem. Toxicol* **2014,** *65*, 129-139.

7. Suzuki, I.; Cone, R. D.; Im, S.; Nordlund, J.; Abdel-Malek, Z. A., Binding of melanotropic hormones to the melanocortin receptor MC1R on human melanocytes stimulates proliferation and melanogenesis, *Endocrinology* **1996,** *137* (5), 1627-1633.
8. Valverde, P.; Healy, E.; Jackson, I.; Rees, J. L.; Thody, A. J., Variants of the melanocyte–stimulating hormone receptor gene are associated with red hair and fair skin in humans, *Nature Genetics* **1995,** *11* (3), 328-330.
9. Nouri, K.; Bowes, L.; Chartier, T.; Romagosa, R.; Spencer, J., Combination Treatment of Melasma with Pulsed CO_2 Laser Followed by Q-Switched Alexandrite Laser: A Pilot Study, *Dermatol. Surg.* **1999,** *25* (6), 494-497.
10. Draelos, Z. D., Skin lightening preparations and the hydroquinone controversy, *Dermatol Ther.* **2007,** *20* (5), 308-313.
11. Lim, J. T. E.; Frcpi; Fams, Treatment of Melasma Using Kojic Acid in a Gel Containing Hydroquinone and Glycolic Acid, *Dermatol. Surg.* **1999,** *25* (4), 282-284.
12. Fan, H.; Liu, G.; Huang, Y.; Li, Y.; Xia, Q., Development of a nanostructured lipid carrier formulation for increasing photo-stability and water solubility of Phenylethyl Resorcinol, *Appl. Surf. Sci.* **2014,** *288*, 193-200.
13. Chang, T. S., An updated review of tyrosinase inhibitors, *Int. J. Mol. Sci.* **2009,** *10* (6), 2440-75.
14. Kim, B.-S.; Na, Y.-G.; Choi, J.-H.; Kim, I.; Lee, E.; Kim, S.-Y.; Lee, J.-Y.; Cho, C.-W., The Improvement of Skin Whitening of Phenylethyl Resorcinol by Nanostructured Lipid Carriers, *Nanomaterials* **2017,** *7*, 241.
15. Yi, X.; Zhao, G.; Zhang, H.; Guan, D.; Meng, R.; Zhang, Y.; Yang, Q.; Jia, H.; Dou, K.; Liu, C.; Que, F.; Yin, J. Q., MITF-siRNA Formulation Is a Safe and Effective Therapy for Human Melasma, *Mol. Ther* **2011,** *19* (2), 362-371.
16. Chen, M.; Zakrewsky, M.; Gupta, V.; Anselmo, A. C.; Slee, D. H.; Muraski, J. A.; Mitragotri, S., Topical delivery of siRNA into skin using SPACE-peptide carriers, *J. Control. Release* **2014,** *179*, 33-41.
17. Barua, S.; Mitragotri, S., Challenges associated with penetration of nanoparticles across cell and tissue barriers: A review of current status and future prospects, *Nano Today* **2014,** *9* (2), 223-243.
18. Carter, P.; Narasimhan, B.; Wang, Q., Biocompatible nanoparticles and vesicular systems in transdermal drug delivery for various skin diseases, *Int. J. Pharm.* **2019,** *555*, 49-62.
19. Lopez, R. F. V.; Seto, J. E.; Blankschtein, D.; Langer, R., Enhancing the transdermal delivery of rigid nanoparticles using the simultaneous application of ultrasound and sodium lauryl sulfate, *Biomaterials* **2011,** *32* (3), 933-941.
20. Zheng, D.; Giljohann, D. A.; Chen, D. L.; Massich, M. D.; Wang, X.-Q.; Iordanov, H.; Mirkin, C. A.; Paller, A. S., Topical delivery of siRNA-based spherical nucleic acid nanoparticle conjugates for gene regulation, *Proc. Natl. Acad. Sci. U.S.A.* **2012,** *109* (30), 11975.
21. Liu, H.; Kang, R. S.; Bagnowski, K.; Yu, J. M.; Radecki, S.; Daniel, W. L.; Anderson, B. R.; Nallagatla, S.; Schook, A.; Agarwal, R.; Giljohann, D. A.; Paller, A. S., Targeting the IL-17 Receptor Using Liposomal Spherical Nucleic Acids as Topical Therapy for Psoriasis, *J. Invest. Dermatol* **2020,** *140* (2), 435-444.e4.
22. Tan, X.; Li, B. B.; Lu, X.; Jia, F.; Santori, C.; Menon, P.; Li, H.; Zhang, B.; Zhao, J. J.; Zhang, K., Light-Triggered, Self-Immolative Nucleic Acid-Drug Nanostructures, *J. Am. Chem. Soc.* **2015,** *137* (19), 6112-6115.
23. Tan, X.; Lu, X.; Jia, F.; Liu, X.; Sun, Y.; Logan, J. K.; Zhang, K., Blurring the Role of Oligonucleotides: Spherical Nucleic Acids as a Drug Delivery Vehicle, *J. Am. Chem. Soc.* **2016,** *138* (34), 10834-10837.
24. Prigodich, A. E.; Alhasan, A. H.; Mirkin, C. A., Selective Enhancement of Nucleases by Polyvalent DNA-Functionalized Gold Nanoparticles, *J. Am. Chem. Soc.* **2011,** *133* (7), 2120-2123.
25. Li, D.; Taylor, A. W., Diminishment of alpha-MSH anti-inflammatory activity in MC1r siRNA-transfected RAW264.7 macrophages, *J Leukoc Biol* **2008,** *84* (1), 191-8.
26. Seong, I.; Min, H. J.; Lee, J. H.; Yeo, C. Y.; Kang, D. M.; Oh, E. S.; Hwang, E. S.; Kim, J., Sox10 controls migration of B16F10 melanoma cells through multiple regulatory target genes, *PLOS ONE* **2012,** *7* (2), e31477.
27. Chung, H.; Lee, J. H.; Jeong, D.; Han, I. O.; Oh, E. S., Melanocortin 1 receptor regulates melanoma cell migration by controlling syndecan-2 expression, *J. Biol. Chem.* **2012,** *287* (23), 19326-35.
28. Lu, X.; Jia, F.; Tan, X.; Wang, D.; Cao, X.; Zheng, J.; Zhang, K., Effective Antisense Gene Regulation via Noncationic, Polyethylene Glycol Brushes, *J. Am. Chem. Soc.* **2016,** *138* (29), 9097-9100.
29. Deng, Z.; Hu, J.; Liu, S., Disulfide-Based Self-Immolative Linkers and Functional Bioconjugates for Biological Applications, *Macromol. Rapid Commun.* **2020,** *41* (1), 1900531.
30. Choi, C. H. J.; Hao, L.; Narayan, S. P.; Auyeung, E.; Mirkin, C. A., Mechanism for the endocytosis of spherical nucleic acid nanoparticle conjugates, *Proc. Natl. Acad. Sci. U.S.A.* **2013,** *110* (19), 7625.
31. Zhang, Y.; Sil, B. C.; Kung, C. P.; Hadgraft, J.; Heinrich, M.; Sinko, B.; Lane, M. E., Characterization and topical delivery of phenylethyl resorcinol, *Int. J. Cosmet. Sci.* **2019,** *41* (5), 479-488.
32. Nordlund, J. J.; Collins, C. E.; Rheins, L. A., Prostaglandin E2 and D2 but Not MSH Stimulate the Proliferation of Pigment Cells in the Pinnal Epidermis of the DBA/2 Mouse, *J. Invest. Dermatol* **1986,** *86* (4), 433-437.
33. Kumar, K. J.; Vani, M. G.; Wang, S. Y.; Liao, J. W.; Hsu, L. S.; Yang, H. L.; Hseu, Y. C., In vitro and in vivo studies disclosed the depigmenting effects of gallic acid: a novel skin lightening agent for hyperpigmentary skin diseases, *BioFactors (Oxford, England)* **2013,** *39* (3), 259-70.
34. Schallreuter, K. U.; Kothari, S.; Chavan, B.; Spencer, J. D., Regulation of melanogenesis – controversies and new concepts, *Exp Dermatol* **2008,** *17* (5), 395-404.

TOC

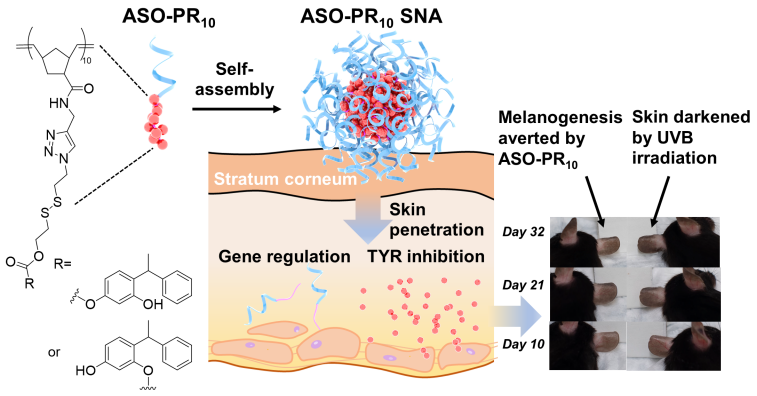

Supporting Information

Spherical nucleic acids for topical treatment of hyperpigmentation

Yang Fang, Xueguang Lu, Dali Wang, Jiansong Cai, Yuyan Wang, Peiru Chen, Mengqi Ren, Hao Lu, Jennifer Union, Lei Zhang, Yehui Sun, Fei Jia, Xi Kang, Xuyu Tan[1,2]*, and Ke Zhang[1]*

1. Department of Chemistry and Chemical Biology, Northeastern University, Boston, Massachusetts 02115, United States

2. Department of Chemistry, Massachusetts Institute of Technology, 77 Massachusetts Avenue, Cambridge, Massachusetts 02139, United States

* Corresponding e-mail: k.zhang@northeastern.edu

Materials and methods

Phosphoramidites and supplies for DNA synthesis were purchased from Glen Research Co., USA. B16F10 cell line was purchased from American Type Culture Collection (Rockville, MD, USA). All other common materials were obtained from Sigma-Aldrich Co. USA, Fisher Scientific Inc., USA, or VWR International LLC., USA, and were used as received unless otherwise indicated. DLS and zeta potential data were recorded on a Malvern Zetasizer Nano-ZSP (Malvern, UK). LC-MS measurements were performed on an Agilent 1260 infinity binary liquid chromatograph coupled to an Agilent 6120 quadrupole mass spectrometer. Sample solution was injected into an Agilent ZORBAX Eclipse XDB-C18, 5μm, 80Å, 50 × 0.5 mm column set at 35 °C (Agilent Technologies, Inc., CA, USA). Fluorescence measurement was carried out on a Cary Eclipse fluorescence spectrophotometer (Varian Inc., CA, USA). ^{1}H and ^{13}C NMR spectra were acquired on Varian 500 or 400 MHz NMR spectrometers (Varian Inc., CA, USA). Chemical shifts (δ) were reported in ppm. Reverse-phase HPLC was performed on a Waters (Waters Co., MA, USA) Breeze 2 HPLC system coupled to a Symmetry® C18 3.5 μm, 4.6×75 mm reversed-phase column and a 2998 PDA detector, using TEAA buffer (0.1 M) and HPLC-grade acetonitrile as mobile phases. *N,N*-Dimethylformamide (DMF) GPC was carried out on a TOSOH EcoSEC HLC-8320 GPC system (Tokyo, Japan) equipped with a TSKgel Alpha-M, 7.8 mm ID ×30 cm column and RI/UV-Vis detectors. HPLC-grade DMF with 0.05 M LiBr was used as the mobile phase and samples were run at a flow rate of 0.4 mL/min. TEM samples were imaged on a JEOL JEM 1010 electron microscope utilizing an accelerating voltage of 80 kV. Gel electrophoresis was performed using 2% agarose gel in 0.5× tris/borate/EDTA (TBE) buffer with a running voltage of 120 V. Gel images were acquired on an Alpha Innotech Fluorochem Q imager.

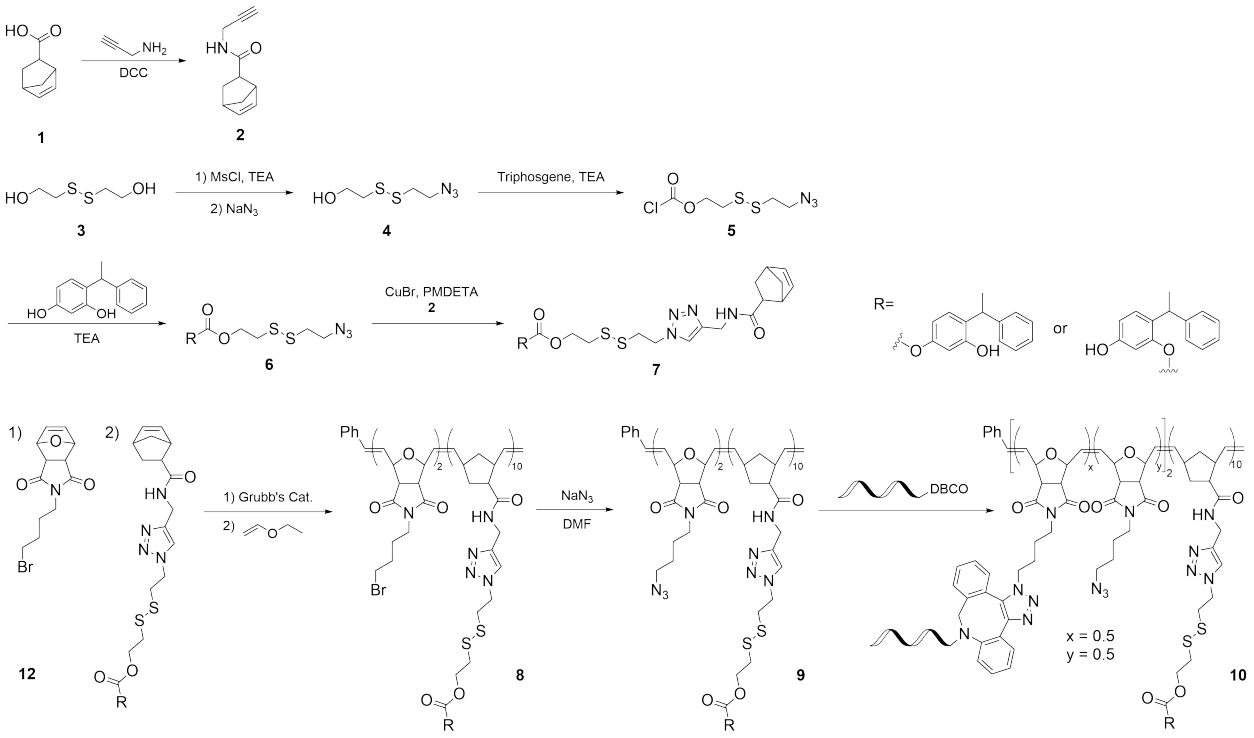

Scheme S1. Synthesis of ASO-PR$_{10}$ amphiphile

Synthesis of compound 6

Compound **5** was synthesized following previously reported protocols.[1] To synthesize **6**, phenylethyl resorcinol (0.32 g, 1.494 mmol) was dissolved in 4 mL of CH_2Cl_2 solution followed by the addition of 3 mL of CH_2Cl_2 containing triethylamine (208 μL, 151.2 mg, 1.50 mmol), and the mixture was placed in ice bath. Compound 5 (0.30g, 1.25 mmol) dissolved in 10 mL of CH_2Cl_2 was added dropwise to the mixture. The reaction mixture was stirred in ice bath for 2 h, then at RT overnight. The crude mixture was diluted with 20 mL of CH_2Cl_2 and rinsed with water (2×30 mL) and

brine (1×30 mL). The organic layer was collected, and solvent was removed under reduced pressure. The crude product was purified by silica gel column chromatography (Hex: EtOAc = 5:1 to 2:1, v:v) to give **6** as a pale yellow oil (0.23 g, 44.1% yield). ^{1}H-NMR (500 MHz, $CDCl_3$): δ 7.17-7.35 (m, 6H), 6.75-6.82 (m, 1H), 6.64-6.67 (m, 1H), 4.50-4.56 (dt, *J* = 11.4, 5.7 Hz, 2H), 4.32-4.29 (dd, *J* = 10.5, 3.5 Hz, 1H), 3.60-3.66 (t, *J* = 6.7 Hz, 2H), 3.04-3.11 (dt, *J* = 13.2, 6.5 Hz, 2H), 2.88-2.94 (dd, *J* = 14.1, 6.9 Hz, 2H), 1.62-1.66 (d, *J* = 7.4 Hz, 3H); ^{13}C NMR (400 MHz, $CDCl_3$) δ 154.07, 153.44, 149.72, 145.20, 130.48, 128.41, 128.38, 128.30, 127.48, 127.48, 126.19, 112.48, 108.56, 66.16, 49.80, 37.91, 37.49, 36.86, 20.83.

Synthesis of monomer 7

Compound **2** was synthesized following previously reported method.[1] Compound **2** (221 mg, 1.26 mmol) and CuBr (136 mg, 0.95 mmol) were added to a 25 mL Schlenk flask. The flask was sealed and purged with N_2 gas three times. Compound **6** (264 mg, 0.63 mmol) was dissolved in 5 mL of deoxygenated CH_2Cl_2, and *N*,*N*′,*N*″,*N*‴-pentamethyldiethylenetriamine (PMDETA, 596 μL, 493 mg, 2.85 mmol) was dissolved in 7 mL of CH_2Cl_2. The two solutions were each placed in a 10 mL Schlenk flask, and three rounds of freeze-pump-thaw cycles were applied. The solutions containing compound **6** and PMDETA were then extracted with a syringe and injected into the flask containing compound **2** and CuBr. The reaction mixture was stirred at RT for 1.5 h. The crude mixture was diluted with 10 mL of CH_2Cl_2 and then rinsed with water (2 × 30 mL) and brine (1 × 30 mL). The organic layer was collected, and solvent was removed under reduced pressure. The crude product was purified by silica gel column chromatography (Hex: EtOAc=1:1, v:v) to give **7** as a white solid (157 mg, 42 % yield). Molecular mass was measured by LC-MS (Figure S13). ^{1}H-NMR (500 MHz, $CDCl_3$): δ 8.65 (s, 1H), 7.64 (s, 1H), 7.32-7.31 (m, 4H), 7.15-7.19 (m, 1H), 7.09-7.14 (d, *J* = 8.5 Hz, 1H), 6.88-6.91 (t, *J* = 2.5 Hz, 1H), 6.63-6.67 (dd, *J* = 8.3, 2.4 Hz, 1H), 6.21 (s, 1H), 6.10-6.14 (m, 1H), 6.03-6.17 (m, 1H), 4.58-4.63 (m, 2H), 4.51-4.56 (q, *J* = 7.1 Hz, 1H), 4.46-4.50 (t, *J* = 5.8 Hz, 2H), 4.42-4.46 (dd, *J* = 5.9, 3.3 Hz, 2H), 3.20-3.26 (t, *J* = 7.3 Hz, 2H), 3.03-3.08 (t, *J* = 5.7 Hz, 2H), 2.85-2.92 (d, *J* = 10.0 Hz, 2H), 1.93-1.99 (m, 1H), 1.81-1.87 (m, *J* = 19.4 Hz, 1H), 1.68-1.64 (m, *J* = 7.1 Hz, 4H), 1.31-1.36 (m, 2H); ^{13}C NMR (400 MHz, $CDCl_3$) δ 176.39, 154.97, 153.56, 149.62, 145.90, 144.77, 138.18, 135.92, 131.22, 128.23 (3C), 127.69 (2C), 125.91, 123.04, 111.40, 108.47, 65.62, 49.53, 46.95, 46.36, 44.52, 41.56, 38.52, 38.46, 37.53, 34.72, 30.52, 20.82.

Synthesis of compound 9

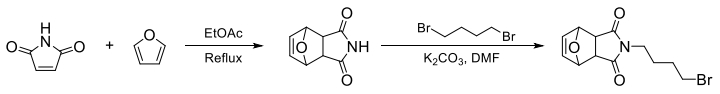

11 **12**

Norbornenyl bromide (compound **12**) was synthesized following previously published method.[2] Compound **12** (2 equiv.) was dissolved in anhydrous CH_2Cl_2 and placed in a Schlenk flask under N_2, which was then vacuumed and purged with N_2 gas three times. The flask was submerged in ice water, before a solution of Grubbs' catalyst 3rd generation (1 equiv.) in deoxygenated CH_2Cl_2 was rapidly added by gastight syringe. The reaction mixture was stirred for 30 min followed by addition of a CH_2Cl_2 solution containing monomer **7** (10 equiv.) with a gastight syringe. The reaction mixture was further stirred for 1 h at 0 °C. Thereafter, several drops of ethyl vinyl ether (EVE) was added into the Schlenk flask and the reaction mixture was further stirred for 30 min. The mixture was then concentrated and precipitated (3×) into 15 mL cold diethyl ether to give a white solid (polymer **8**). The polymer was dried under high vacuum, redissolved in DMF, and mixed with an excess of sodium azide while stirring. After overnight reaction at RT, the solution was dialyzed against Nanopure™ water for 24 h, and the resulting liquid-solid dispersion was dried by lyophilization to give polymer **9**.

Synthesis and purification of ASO-PR$_{10}$ conjugate

Polymer **9** (1.3 mg, 200 nmol) was dissolved in 200 μL of DMF and DBCO-modified DNA (100 nmol) was dissolved in 40 μL of water. The two solutions were mixed, and the reaction mixture was gently shaken on an Eppendorf Thermomixer at 50 °C for 48 h. The mixture was then dialyzed against Nanopure™ water for 24 h to remove DMF, and the dialysate was centrifuged at 14,000 rpm for 10 min to remove unreacted polymer. Thereafter, the supernatant was collected and electrophoresed under the voltage of 120 V in 2% agarose gel (buffer: 0.5 × Tris-Borate-EDTA, TBE). The electrophoresis was stopped when the unreacted DNA and conjugated DNA showed clear separation, then the band containing ASO-PR$_{10}$ was cut and further electroeluted by using dialysis tubing with a MWCO of 6-8 kDa.

The electroeluted solution was further dialyzed against Nanopure™ water overnight to remove impurities. The dialysate was collected and concentrated using a Spin-X® UF Concentrator (MWCO 30 kDa, Corning). PR-devoid micelles were acquired by treating the ASO-PR_{10} with 10 mM DTT at 37 °C overnight, followed by dialysis in Nanopure™ for 24 h to remove small molecular residues.[1] The concentration of the micelles are determined by measuring DNA UV-Vis absorption at 260/280 nm.

Quantification of ASO-PR_{10}

Due to the fact that PR exhibit certain absorbance at 260 nm, the typical optical quantification method for determining DNA concentration needs to be modified. In order to establish the concentration of ASO-PR_{10}, Cy5-labeled conjugate was subjected to prolonged nuclease treatment (DNase I, 12 h, Sigma Aldrich) to fully release Cy5. The released dye was compared to a standard curve established with sulfo-Cy5 NHS ester. The calculated concentration of the conjugate is then correlated to its absorbance at 260 nm (1.0 $OD_{260\ nm}$ = 1.04 μM, Figure S14).

Cell culture

B16F10 murine melanoma cells were cultured in Dulbecco's modified Eagle's medium- high glucose (DMEM, Sigma Aldrich) supplied with 10% fetal bovine serum (FBS), 100 units/mL penicillin, and 100 μg/mL streptomycin at 37 °C in a humidified atmosphere containing 5% CO_2. The culture medium was changed every two days. The cells were harvested with 0.25% trypsin and 2.21mM EDTA through trypsinization.

MTT assay

Cell viability was measured by using the 3-(4,5-dimethylthiazol-2-yl)-2,5 diphenyltetrazolium bromide (MTT) assay. Briefly, B16F10 cells were seeded into 96-well plates at 2,000 cells per well in 200 μL of full-growth medium and cultured overnight. For ASO-PR_{10}-treated cells: after removing the medium, the cells were rinsed with phosphate buffered saline (PBS) 3× and then treated with ASO-PR_{10} at various concentrations (1 to 20 μM, PR basis) in serum-free medium at 37 °C for 6 h. Then, 100 μL of full-growth medium was added and the cells were further incubated for 42 h. For PR-treated cells: cells were treated with PR with various concentrations (1 to 20 μM) in 200 μL of full-growth medium and incubated for 48 h. After incubation, 10 μL of MTT solution (5 mg/mL in PBS) was added to each well. The cells were further incubated for another 4 h before the medium was removed. Then, 100 μL of DMSO was added to each well, and the culture plate was gently shaken for 10 min to completely dissolve blue formazan crystals. The assay was conducted in quadruplicate and each experiment was repeated three times. Cell viability was determined by measuring the absorbance of formazan at 560 nm using a BioTek® Synergy™ Neo2 Multi-Mode microplate reader (BioTek Inc., VT, USA).

Flow cytometry

B16F10 cells were seeded into 24-well plates at 1.0×10^5 cells per well in 1 mL of full-growth medium and cultured overnight at 37 °C with 5% CO_2. After removing the medium, the cells were rinsed with PBS 3× and then serum-free medium containing Cy5-labeled ASO-PR_{10} nanoparticles or Cy5-labeled free DNA with varying doses (0.2 to 2 μM, DNA basis) were added to each well. The cells were then further incubated at 37 °C for 4 h. Subsequently, medium was removed, the cells were rinsed with PBS 3×, trypsinized, centrifuged, and re-suspended in 600 μL of fresh PBS. All samples were analyzed by flow cytometry (Attune NxT, Invitrogen, CA, USA) to determine the extent of cell uptake. The experiment was repeated three times.

Confocal laser scanning microscopy

To visualize the cell uptake of ASO-PR_{10}, B16F10 cells were seeded in 24-well glass bottom plates at a density of 1.0×10^5 cells per well and were cultured overnight in 1 mL of full-growth medium at 37 °C in 5% CO_2 atmosphere. After removing the medium, the cells were rinsed with PBS 3× and then serum-free medium containing Cy5-labeled ASO-PR_{10} or free DNA (2 μM, DNA basis) was added to the well. The cells were then incubated at 37 °C for 4 h, before being rinsed with PBS 3×, fixed with 4% paraformaldehyde for 30 min, and rinsed again with PBS 3×. Cells were stained with Hoechst 33342 for 10 min and imaged on an LSM-700 confocal laser scanning microscope (Carl Zeiss Ltd., Cambridge, UK). Imaging settings were kept identical for all samples in each study.

Chemical blocking of cell uptake

B16F10 cells were seeded into 24-well plates at 1.0×10^5 cells per well in 1 mL of full-growth medium and cultured overnight at 37 °C with 5% CO_2. After removing the medium, cells were pretreated with 400 μL of serum-free medium that contains methyl β-cyclodextrin (MβCD, 12.5 mg/mL) per well for 30 min. 10 μL of Cy5-labeled ASO-PR_{10} was

added to each well to a final concentration of 300 nM (ASO basis), and cells were incubated for another 4 h. To visualize the extent of blocking, cells were stained and imaged on an LSM-700 confocal laser scanning microscope with the same procedure provided above.

Cellular tyrosinase inhibition assay

The activity of cellular tyrosinase was evaluated by measuring the rate of oxidation of L-DOPA based on a method described previously with minor modifications.[3] Briefly, B16F10 cells were seeded into 6-well plates at 1.0×10^5 cells per well in 3 mL of full-growth medium and cultured overnight at 37 °C with 5% CO_2 to allow cells to adhere. Then, cells were exposed to 200 nM of alpha-melanocyte stimulating hormone (α-MSH) in 2 mL of full-growth medium for 24 h. The medium was removed and increasing doses of ASO-PR_{10} nanoparticles or PR (2 to 20 μM, PR basis), Scr-PR_{10} (10 μM, PR basis), and PR-devoid micelles (1 μM, ASO basis) dissolved in 1 mL of serum-free medium were added to the wells in the presence of 200 nM of α-MSH. The cells were incubated for 6 h, before 1 mL of full-growth medium containing 200 nM of α-MSH was added. The cells were further cultured for another 42 h, before the activity of cellular tyrosinase was measured. Cells were washed with cold PBS 3 × and lysed with 300 μL of 0.1 M sodium phosphate buffer (pH 6.8) containing 1% Triton X-100 and 5 mM EDTA for 30 min at 0 °C. The lysates were then centrifuged at 21,000 g for 30 min at 4 °C. After centrifugation, the protein concentration of resulting supernatant was determined by a bicinchoninic acid (BCA) protein assay with bovine serum albumin (BSA) as the protein standard. Next, a freshly prepared substrate solution of 0.1% L-DOPA (50 μL) was added to 40 μg of protein. The reaction volume was adjusted to 150 μL with 0.1 M sodium phosphate buffer pH (6.8). Then, 100 μL of each reaction mixture was transferred to a 96-well plate and allowed to incubation at 37 °C for 1 h. Tyrosinase activity was quantified by measuring the absorbance at 475 nm using a microplate reader, and enzyme activity was calculated using the following equation:

$$\text{Tyrosinase activity (\%)} = (OD_{sample}\text{-}OD_{blank})/(OD_{control}\text{-}OD_{blank}) \times 100\%$$

Melanin content assay

Cell culture and sample treatment procedures were identical to that of the tyrosinase inhibition assay. Cells were rinsed with PBS 3×, detached by incubation with trypsin-EDTA, and centrifuged at 1,000 rpm for 10 min. Then, the medium was discarded, and pellets were washed with 500 μL of PBS and collected by centrifugation (1,000 rpm,10 min). The pellets were placed in 1 N NaOH containing 10% DMSO for 1 h at 80 °C to dissolve the melanin. 100 μL of each solution were transferred to a 96-well plate, and the melanin content was measured against an authentic standard of synthetic melanin by measuring the absorbance at 405 nm (Figure S15). The protein concentration was quantified by a bicinchoninic acid (BCA) protein assay with BSA as the protein standard. The specific melanin content was normalized to the total protein concentration in the same sample and shown as Total melanin/Total protein (μg/μg).

Western blotting

B16F10 cells were seeded into 12-well plates at 1.0×10^5 cells per well in 2 mL of full-growth medium and cultured overnight at 37 °C with 5% CO_2. Cells were then incubated with Lipofectamine2k-complexed DNA (10 μM), ASO-PR_{10}, or PR at various concentration (2 to 20 μM, PR basis) in 1mL of serum-free medium for 6 h. Thereafter, 1 mL of full-growth medium was added into the wells and cells were further cultured for another 66 h. Whole cell lysate was collected in 100 μL of radioimmunoprecipitation assay cell lysis buffer (RIPA) mixed with Halt™ (1× Protease and Phosphatase Inhibitor Cocktail and 5 mM of EDTA, ThermoFisher, MA, USA). Protein concentrations were determined by a BCA protein assay with BSA as the protein standard. Equal amounts (35 μg) of protein samples were separated by 4-20% SDS-PAGE, electro-transferred to nitrocellulose membrane, and blocked for 1 h at RT with 3% BSA in tris-buffered saline supplemented with 0.05% Tween 20. The membrane was then incubated with primary antibodies against α-tubulin (1:2000 dilution, Cell Signaling Technology, MA, USA) and MC1R (1:1000 dilution, Invitrogen, CA, USA) at 4°C overnight followed by incubation with secondary antibodies (1:5000 dilution, Cell Signaling Technology, MA, USA) at RT for 1 h. Protein bands were visualized by using an ECL Western Blotting Substrate (Pierce, ThermoFisher, MA, USA).

Topical treatment in UVB-irradiated mouse ear skin model

The experimental process is based upon a previously described method with modifications.[4] Animal protocols were approved by the Institutional Animal Care and Use Committee of Northeastern University and were carried out in accordance with the approved guidelines. Six-week-old female C57BL/6 mice were divided into three groups: ASO-PR_{10}, PR, and control. The ASO-PR_{10} nanoparticles were formulated as a 10 μM aqueous solution in Nanopure™

water, while PR was formulated as a 100 μM solution in 1,2-propanediol/ethanol (v/v 3:7). The concentration difference is to ensure each sample contains the same dose of PR. The hair on the dorsal ear skin was removed on day 0. On days 1-7, mice were treated with samples daily but not UVB irradiation. In order to rule out differences among individuals, the left dorsal ear skin of each mice was topically applied with vehicle only (20 μL of Nanopure™ water or 1,2-propanediol/ethanol) while the right ear was applied with samples (20 μL). On days 8-22, animals in ASO-PR_{10}- and PR-treated groups (including the corresponding vehicle-treated ears) were exposed to UVB irradiation (200 mJ/cm^2) every two days in the morning (8 treatments in total) using a UV lamp (UVP, Inc., CA, USA) with peak emission at 302 nm. During the UVB irradiation, mice were able to move freely. In the afternoon of each day during this period, ASO-PR_{10}, PR, or vehicle were applied to the ear skin. The sample treatment continued from day 23 until day 32, during which period no UVB irradiation was applied. Animals from the control group received neither sample nor UV irradiation. The body weight of the animals was measured once a week (Figure S16).

Measurement of ear skin lightness

The lightness of mouse dorsal ear skin was measured through colorimetry using a tristimulus colorimeter (Colorimeter model WR10QC, China) daily from day 1. The head region of each mice was also photographed under controlled lighting conditions and identical camera settings.

Preparation of skin specimens and Fontana-Masson staining

The mice were euthanized through excess carbon dioxide inhalation at the end of the experiment. Both ears from each mouse were excised, fixed in 10% neutral buffered formalin, and embedded in paraffin for further staining experiments. Paraffin sections were stained for histological visualization of melanin by using a Fontana–Masson staining kit (Abcam, Cambridge, UK) and prepared according to manufacturer's instructions. Briefly, sliced skins were stained with fresh-made ammoniacal silver solution for 30 min at 58-60 °C followed by incubation in 0.2% gold chloride for 30 s, 5% sodium thiosulfate for 1 min, and nuclear fast red solution for 5 min.

Immunohistochemical staining

Immunohistochemistry targeting MC1R protein in the epidermis layer was carried out using rabbit anti-MC1R primary antibody (1:100 dilution, MilliporeSigma, MA, USA) and Cy5-labeled goat anti-rabbit secondary antibody (1:200 dilution, ThermoFisher, MA, USA). Briefly, sliced skins were blocked for 1 h, incubated with the anti-MC1R primary antibody for 2 h, and then incubated with a secondary antibody for 1 h. Samples were stained with Hoechst 33342 for 10 min and imaged on an LSM-700 confocal laser scanning microscope (Carl Zeiss Ltd., Cambridge, UK). Imaging settings were kept identical for all samples.

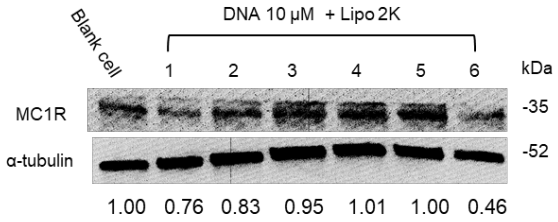

Figure S1. Western blot analysis of cell lysates from B16F10 cells treated with Lipofectamine2k-complexed DNAs for 72 h (DNA strands 1-6, Table S1).

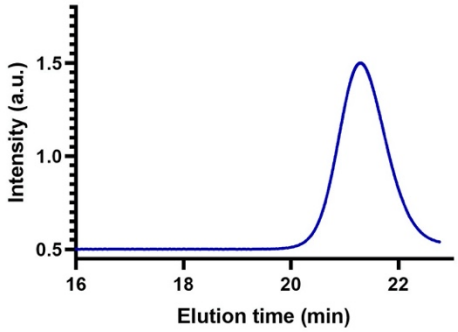

Figure S2. DMF GPC chromatogram of polymer **8**, showing a symmetrical, monomodal peak.

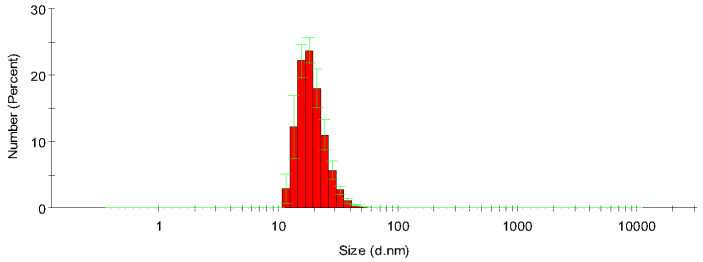

Figure S3. Number-average hydrodynamic diameter of ASO-PR_{10} micelles as determined by DLS.

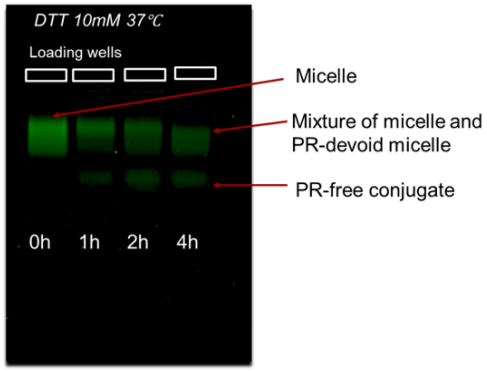

Figure S4. Release of PR from ASO-PR_{10} micelles via bioreductive cleavage of a self-immolative linker by dithiothreitol (10 mM).

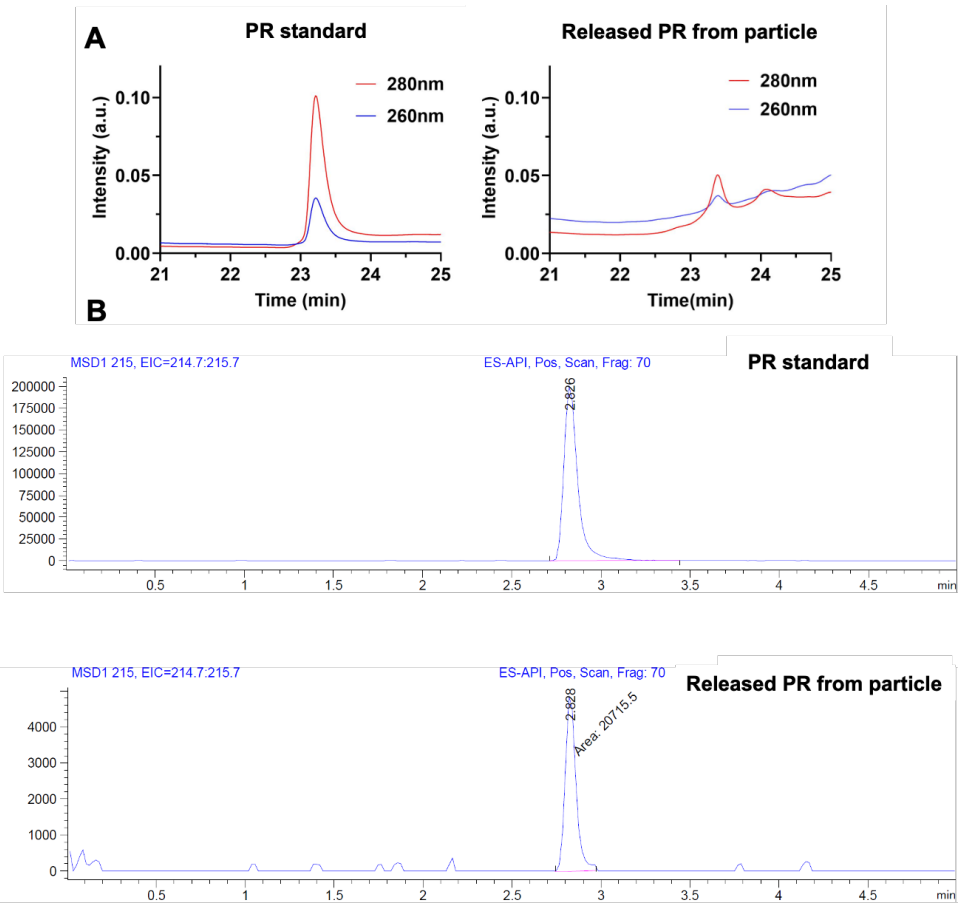

Figure S5. A) Reverse-phase HPLC chromatograms of free PR and PR released from ASO-PR$_{10}$ nanoparticles by treatment with 10 mM DTT for 4h at 37 °C, showing matching retention times. The baseline of particle-release PR is not flat due to PR-devoid polymer appearing as a broad peak from 22-37 min. **B)** LC-MS of free PR and particle-released PR, showing identical elution times and molecular mass as determined by extracted ion chromatogram.

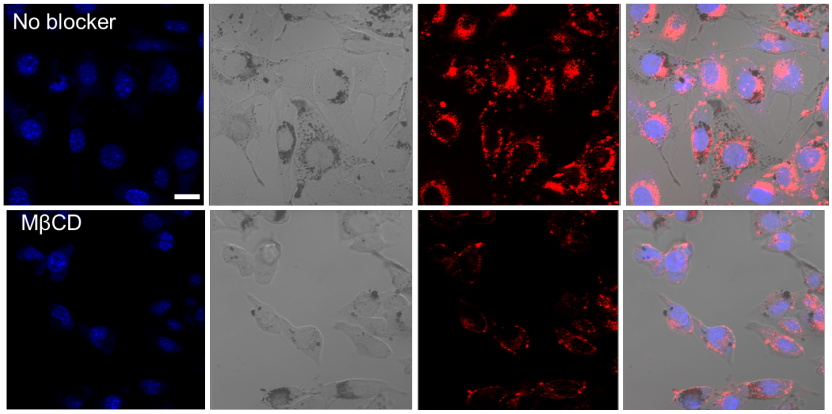

Figure S6. Confocal microscopy imaging of cells pretreated with methyl β-cyclodextrin (MβCD) followed by the treatment of 300 nM of Cy5-labeled ASO-PR$_{10}$ nanoparticles. Images were taken with identical settings. Scale bar: 20 μm.

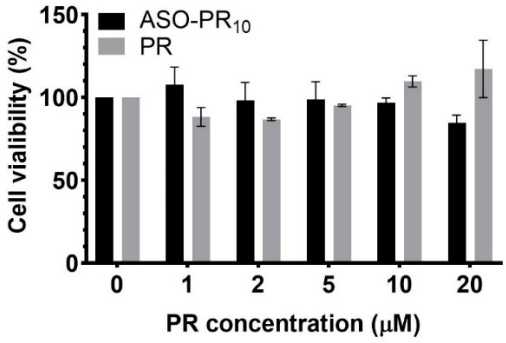

Figure S7. Viability of B16F10 cells treated with PR and ASO-PR$_{10}$, as determined by an MTT cell viability assay.

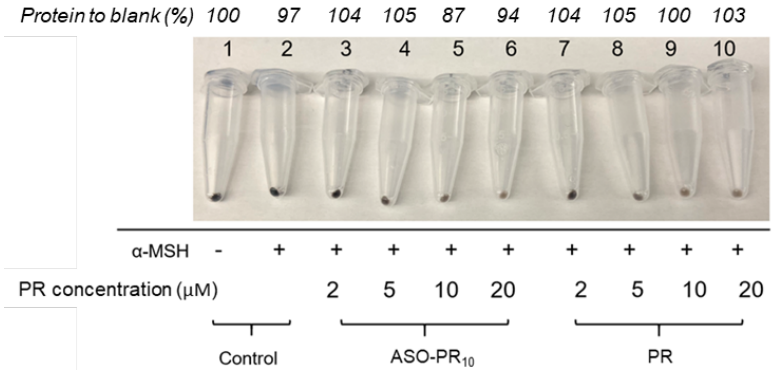

Figure S8. Photograph of pellets of B16F10 cells treated with varying concentrations of PR or ASO-PR$_{10}$ particles. Cells were co-incubated with α-MSH to stimulate melanogenesis. Both free PR and the particles were able to reduce melanin content sufficiently to produce a visible difference in lightness.

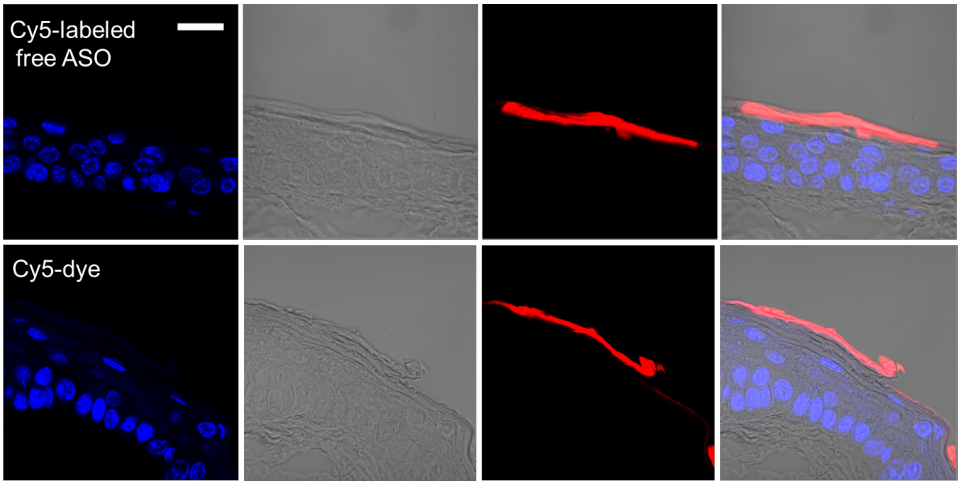

Figure S9. Fluorescence micrographs of mouse ear sections (paraffin-embedded) after treatment with 10 μM Cy5-labeled free ASO or 10 μM Cy5 dye (red). Cell nuclei are stained with Hoechst 33342 (blue). Images were taken with identical settings. Scale bar: 20 μm.

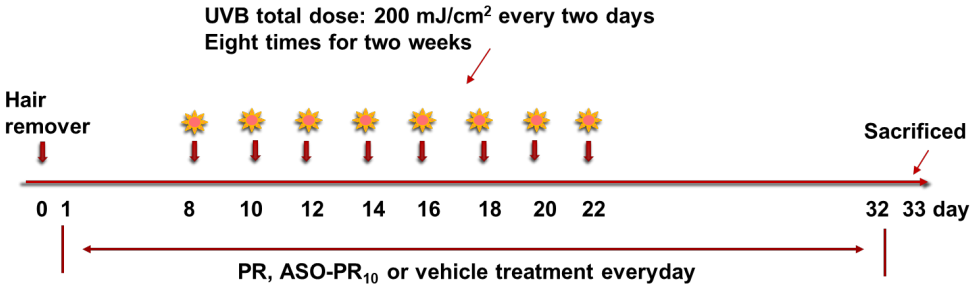

Figure S10. Schedule of treatment for topical application of sample and UVB irradiation in mouse study.

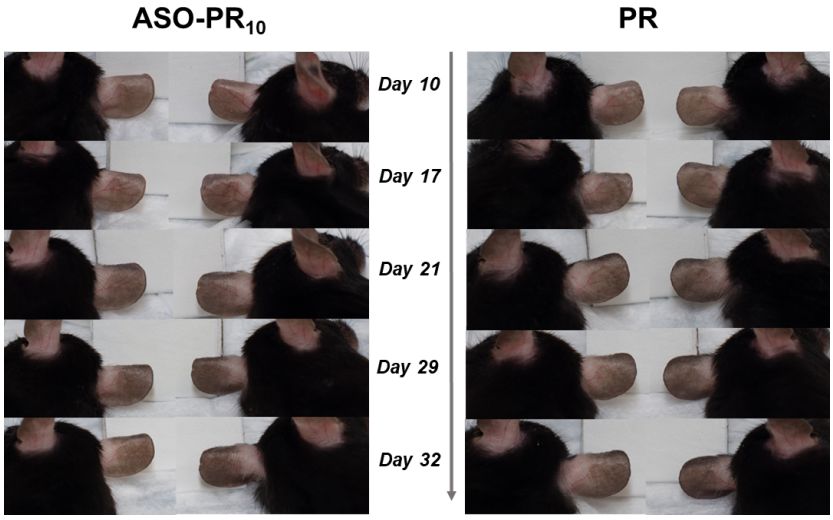

Figure S11. Photograph showing the progression of lightness changes associated with UVB irradiation (left ear) and the protective property of PR and ASO-PR$_{10}$ (right ear) during the 32-day treatment period.

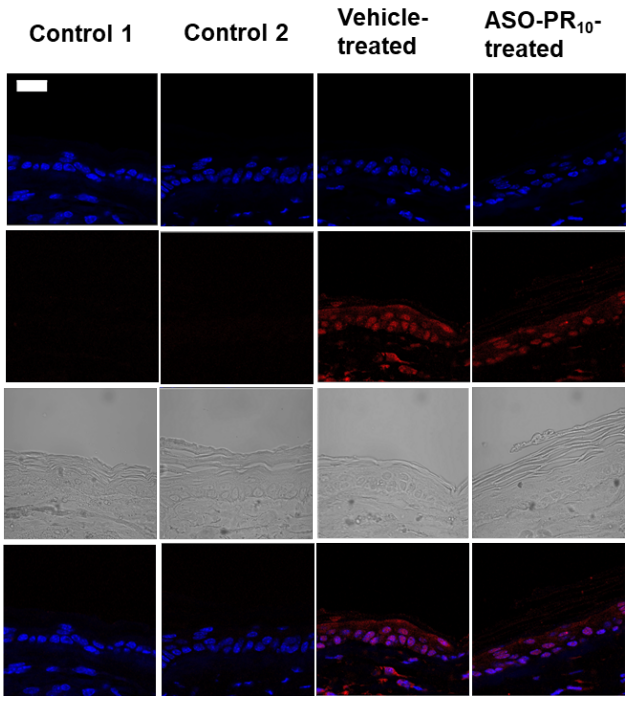

Figure S12. Immunohistostaining of MC1R protein levels (red) in paraffin-embedded mouse ear sections. Controls 1 and 2 are staining controls to rule out non-specific binding. In control 1, a BSA blocking solution was applied to the mouse ear section but no primary or secondary antibodies were used. Control 2 involve the use of a BSA blocking solution lacking the primary antibody but the ear section sample was subsequently treated with a secondary antibody. The ASO-PR_{10}-treated ear exhibit lower intensity in MC1R-related fluorescence compared with vehicle (Nanopure™ water)-treated ear. Scale bar: 20 μm. Cell nuclei are stained with Hoechst 33342 (blue).

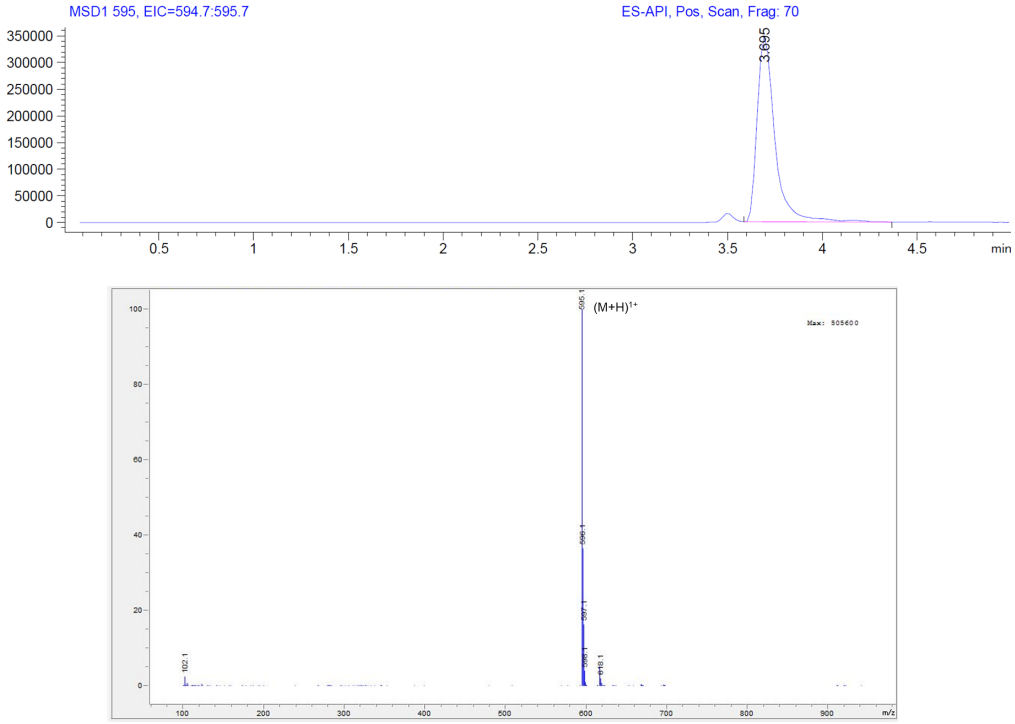

Figure S13. LC chromatogram (top) and extracted ion mass spectrum (bottom) of monomer **7**.

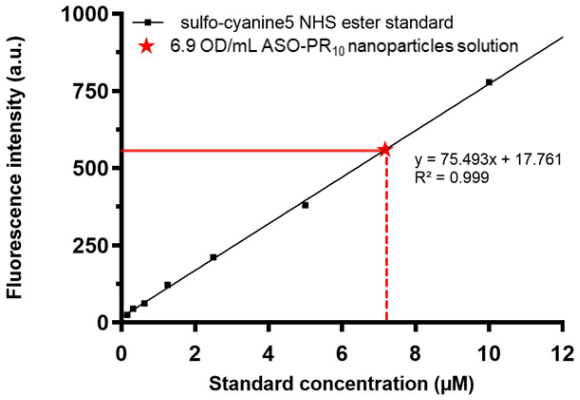

Figure S14. Establishment of the concentration of ASO-PR_{10} nanoparticles (★) using a standard curve generated with sulfo-Cy5 NHS ester.

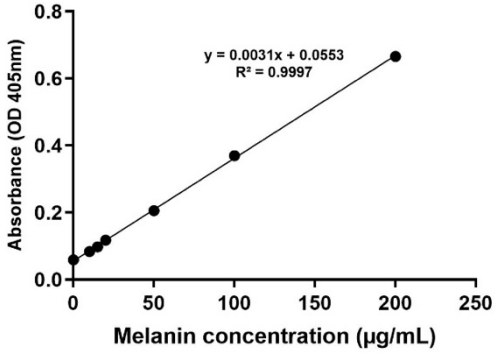

Figure S15. Synthetic melanin standard curve in melanin content assay.

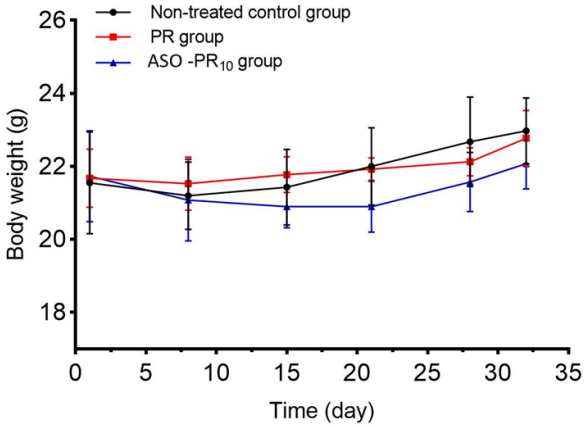

Figure S16. Body weight variation of C57BL/6 mice during the 32-day treatment period.

Table S1. DNA sequences used in this study

Name	Sequence
1	5'-TGATAGTAGTCTCCAGCAC-3'
2	5'- TGCACCAAAGCCACTCTGG-3'
3	5’-CTGGATATCACTGTCACCC-3’
4	5’-TCAGGAAGGGATGAGTACC-3’
5	5’-TCTATTTTAAAGCTCATCC-3’
6	5’-TTCTCCACCAGACTCACCA-3’
7 DBCO modified MC1R antisense	5’-DBCO-TTCTCCACCAGACTCACCA-3’
8 Cy5 and DBCO modified MC1R antisense	5’-DBCO-TTCTCCACCAGACTCACCA-Cy5-3’
9 DBCO modified scramble sequence	5’-DBCO-ACGCAACCTCACTCTTACC -3’

Table S2. Number-average hydrodynamic diameter of ASO-PR_{10}, Scr-PR_{10}, Cy5-labeled ASO-PR_{10}, and PR-devoid micelles as determined by DLS.

Name	Diameter (nm)
ASO-PR_{10}	18.4 ± 5.2
Scr-PR_{10}	18.9 ± 5.5
Cy5-labeled ASO-PR_{10}	19.0 ± 5.5
PR-devoid micelles	17.3 ± 6.2

References

1. Tan, X.; Lu, X.; Jia, F.; Liu, X.; Sun, Y.; Logan, J. K.; Zhang, K., Blurring the Role of Oligonucleotides: Spherical Nucleic Acids as a Drug Delivery Vehicle, *J. Am. Chem. Soc.* **2016,** *138* (34), 10834-10837.
2. Lu, X.; Jia, F.; Tan, X.; Wang, D.; Cao, X.; Zheng, J.; Zhang, K., Effective Antisense Gene Regulation via Noncationic, Polyethylene Glycol Brushes, *J. Am. Chem. Soc.* **2016,** *138* (29), 9097-9100.
3. Kim, B.-S.; Na, Y.-G.; Choi, J.-H.; Kim, I.; Lee, E.; Kim, S.-Y.; Lee, J.-Y.; Cho, C.-W., The Improvement of Skin Whitening of Phenylethyl Resorcinol by Nanostructured Lipid Carriers, *Nanomaterials* **2017,** *7*, 241.
4. You, Y. J.; Wu, P. Y.; Liu, Y. J.; Hou, C. W.; Wu, C. S.; Wen, K. C.; Lin, C. Y.; Chiang, H. M., Sesamol Inhibited Ultraviolet Radiation-Induced Hyperpigmentation and Damage in C57BL/6 Mouse Skin, *Antioxidants (Basel)* **2019,** *8* (7).